Journal of Geophysical Research: Oceans

Supporting Information for

Field measurement and prediction of drag in a planted *Rhizophora* mangrove forest

Masaya Yoshikai[1], Takashi Nakamura[1], Dominic M. Bautista[2], Eugene C. Herrera[2], Alvin Baloloy[3], Rempei Suwa[4], Ryan Basina[5], Yasmin H. Primavera-Tirol[5], Ariel C. Blanco[3], Kazuo Nadaoka[1]

[1]School of Environment and Society, Tokyo Institute of Technology, O-okayama 2-12-1 W8-13 Meguro, Tokyo 152-8552, Japan

[2]Institute of Civil Engineering, University of the Philippines, Diliman, Quezon City 1101, Philippines

[3]Department of Geodetic Engineering, College of Engineering, University of the Philippines, Diliman, Quezon City 1101, Philippines

[4]Forestry Division, Japan International Research Center for Agricultural Sciences (JIRCAS), 1-1 Ohwashi, Tsukuba, Ibaraki 305-8686, Japan

[5]College of Fisheries and Marine Sciences, Aklan State University, New Washington, Aklan, Philippines

Contents of this file

Text S1. Particle tracking velocimetry survey

A particle tracking velocimetry (PTV) survey was conducted on March 20, 2019, during spring tide, to examine the flow field around a reference tree (Fig. 1c). Four downward-looking digital video cameras (RICOH WG-5) were attached on the stem of the reference tree and oriented in such a way that the different camera views covered the entire root system. A pressure sensor was deployed near the reference tree to monitor water depth. Floating particles (represented by leaves of *Moringa oleifera Lam*, 1 cm dimension in average) were prepared prior to the survey. The PTV was conducted twice at different water depths during flood tide (22:00 and 22:40 on March 20, 2019; Fig. S1c). Before releasing the particles, a square scale with known dimension was placed on the water surface seen by each camera view; this was used for image rectification and scaling. The particles were then released, and the movement of particles around the reference tree was monitored by the four video cameras with a rate of 30 frames per second. After the particle release, velocity profiling using an electro-magnetic current meter (AEM213-DA sensor) was conducted at four locations (P1–P4), as performed in the drag survey described in the manuscript. However, note that profiling was not done when the water depth was shallow for the profiling (22:40 on March 20, 2019).

The trajectories of particles were analyzed for each video data using the open-source PTV software TracTrac developed by Heyman (2019). The video data with particle trajectories were rectified and projected to real-world coordinates with a homography matrix determined based on the square scale (Patalano et al., 2017). The projected data from each camera were combined to make one mosaic image with trajectories that covers the entire root system of the tree. The image was partitioned into 10 cm × 10 cm grids, and in each grid, particle displacements per 10 frames ($dt \approx 0.33$ second) were extracted for all particles as displacement samples. The mean particle displacement per dt was calculated by averaging all the displacement samples in a grid, and the mean velocity in the grid was derived from the mean displacement (Fig. S1a–b).

The mean velocities in the grids were averaged, and the major axis component of the averaged velocity was represented as the stream-wise spatially averaged velocity at the water surface, $\langle u \rangle$. The mean velocities of regions where velocity profiling was conducted were also extracted (P1–P4; Fig. S1a–b), and the surface stream-wise velocity averaged for the four locations $\langle u_{p1–4} \rangle$ were likewise derived. The $\langle u_{p1–4} \rangle$ was also estimated from the surface velocities measured by the AEM213-DA sensor. The $\langle u_{p1–4} \rangle$ was then compared with $\langle u \rangle$ to examine the validity of the assumption that the average of the velocities at the four locations, $\langle u_{p1–4} \rangle$, represents the spatial average in the area, $\langle u \rangle$.

The results showed that the $\langle u_{p1–4} \rangle$ derived from PTV and current meter sensor are comparable with values 6.3 cm s^{-1} and 6.6 cm s^{-1}, respectively (Fig. S1d), which ensures a certain accuracy of the PTV-derived velocity field. The comparison with $\langle u \rangle$ showed 10% to 20% deviation of $\langle u_{p1–4} \rangle$ from $\langle u \rangle$. The values of deviation were referred to as errors of estimating the spatially averaged velocity from velocities at the four locations.

Text S2. Acoustic Doppler Velocimeter (ADV) data processing

The velocity data collected by the ADV were despiked using the phase-space method described in Mori et al. (2007). The despiked velocities (eastward, northward, and vertical) were rotated to give the velocities along the *x*, *y*, and *z*-axes, where the instrument tilt was corrected to make the averaged vertical velocity zero (Lee et al., 2004). Bed drag (F_{bed}, m^2 s^{-2}) was then determined from Reynolds stress, ($-\overline{u'w'}$), where u' and w' are the velocity fluctuations of *x*- and *z*-axis components (m s^{-1}), respectively, and the overbar denotes the time average (note that velocities in the equations in the manuscript denote time-averaged values without the overbars).

As shown in Figs. 5b and 5f, the velocity measured by ADV during the flood tides largely deviated from the EM-measured velocity and *U*, possibly due to the local influence of nearby roots. Thus, the Reynolds stress measured during flood tides might have been affected by the wakes generated by the roots aside from the bottom friction. In this regard, we excluded the data during flood tides when estimating the bed drag coefficient.

The estimated drag coefficient, C_{bed}, was 4.2×10^{-3} (Fig. S2). This value is higher but in the same order of magnitude as the drag coefficient observed in muddy tidal environment (e.g., 2.5×10^{-3} in Mariotti and Fagherazzi, 2012).

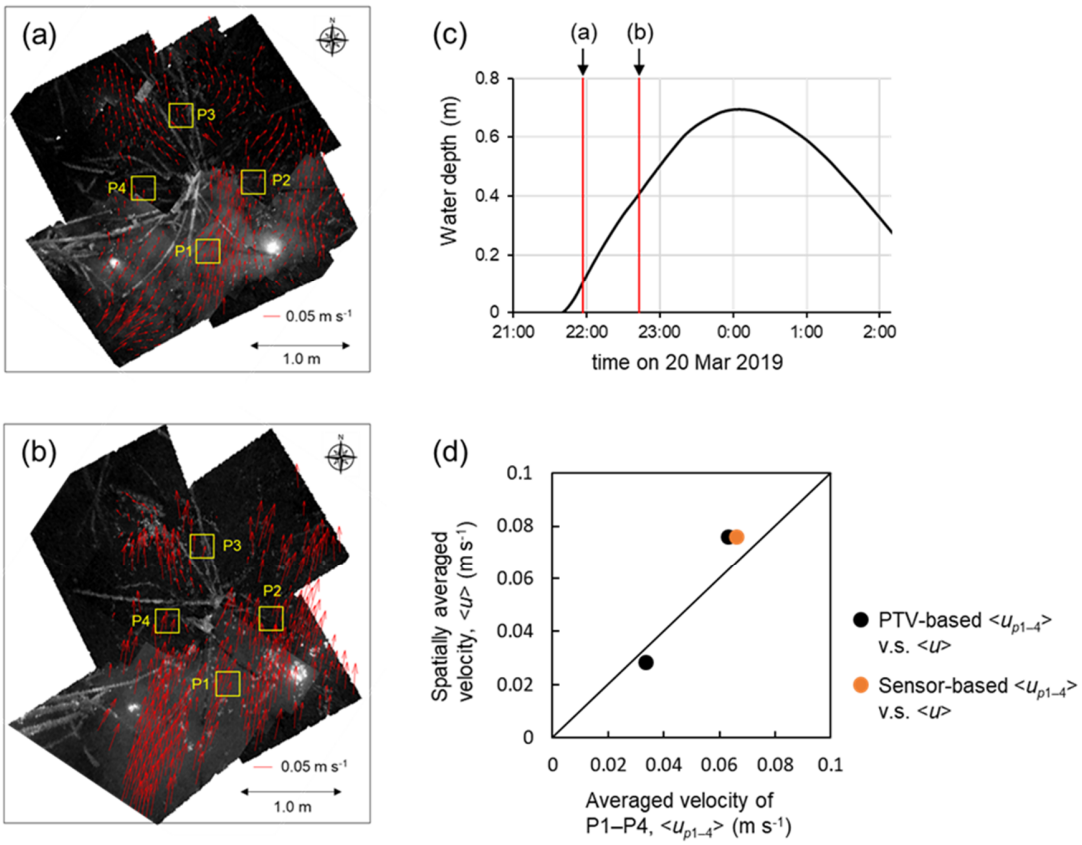

Figure S1. Mean velocity fields around the reference tree at (a) 22:00 and (b) 22:40 on March 20, 2019; (c) time-series data of water depth near the reference tree (the timing when the particles were released are indicated by the red lines); and (d) comparison between $\langle u_{p1\text{–}4} \rangle$ and $\langle u \rangle$.

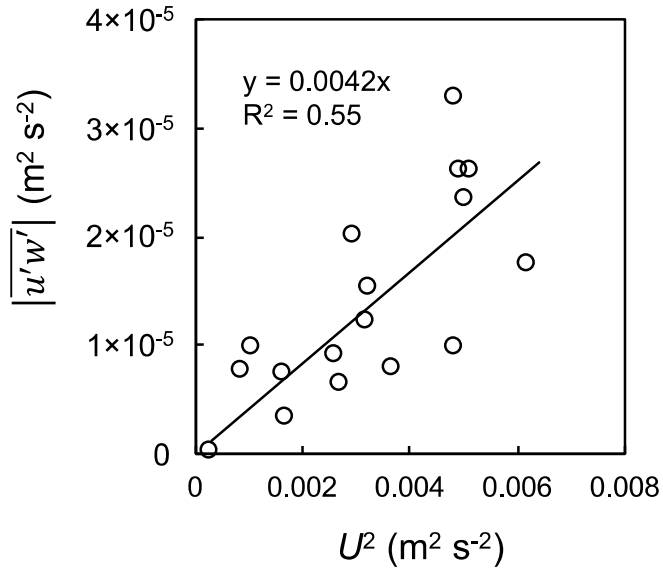

Figure S2. Relationship between U^2 and Reynolds stress $|\overline{u'w'}|$. The slope of the fitted line represents the bed drag coefficient.

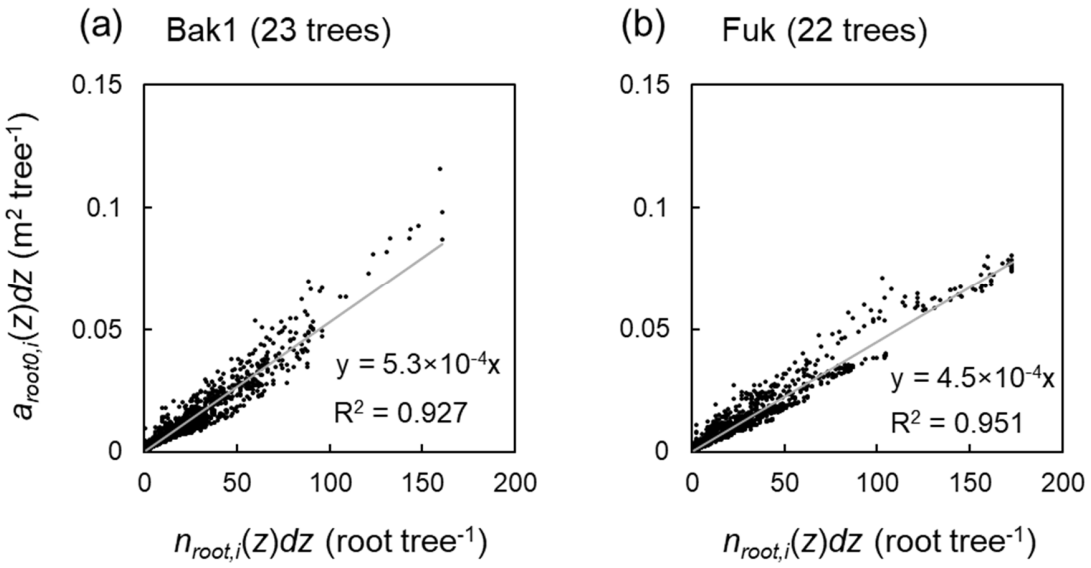

Figure S3. Comparison of number of roots per *dz* per tree, $n_{root,i}(z)$ (root m^{-1} tree^{-1}), and root projected area with zero azimuth angles per *dz* per tree, $a_{root0,i}(z)$ (m tree^{-1}), for (a) our study site for drag measurement (referred to as Bak1 in Yoshikai et al., 2021) and (b) Fukido mangrove forest in Ishigaki Island, Japan (Fuk in Yoshikai et al., 2021). A 0.01-m vertical height interval, *dz*, was used to compute the vertical profiles. Data from 23 trees in Bak1 and 22 trees in Fuk were plotted, respectively.

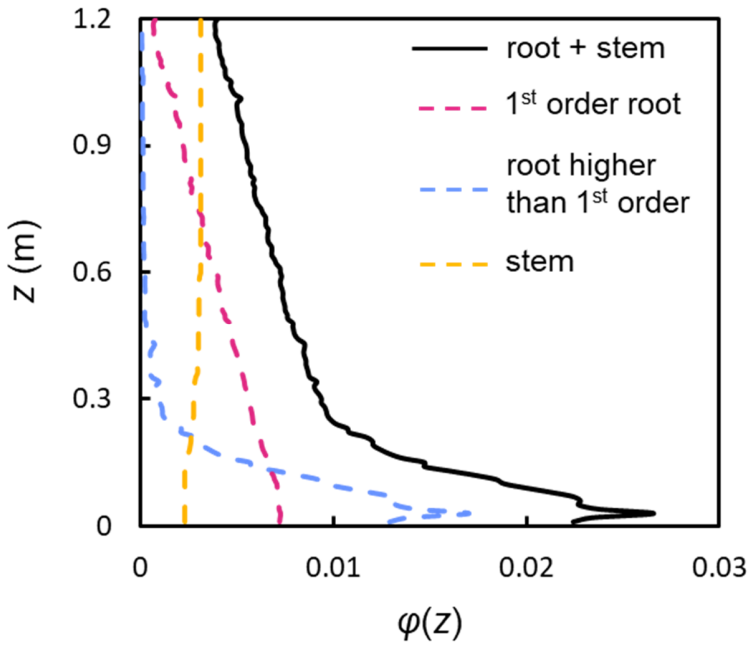

Figure S4. Vertical profile of solid volume fraction (φ, dimensionless), where the values of φ were calculated with 0.01-m vertical resolution. The black solid line shows the solid volume fraction of total vegetation while the red, blue, and yellow dashed lines show the contributions of 1st order root, higher order root, and stem to φ, respectively.